The Origin Of Complex Polarization Behavior In Parsec-scale Jet Knots

Philip Hughes (University of Michigan)

Background: Random Fields – Made to Order

Evidence for random fields in parsec-scale jets:

- Low degree of polarization in a quiescent state; rarely more than ten percent during outbursts – suggests 'root-N' depolarization in a synchrotron source with many randomly oriented magnetic cells.
- Jones et al. (1985) successfully used Monte Carlo simulation to model 'rotator events' as a consequence of a random walk as turbulent field is advected across the observable part of the flow channel.
- Hughes et al. (1989a,b, 1991) and Gómez et al. (1993, 1994a,b) have successfully modeled the temporal, spatial, and spectral attributes of outbursts in a number of individual sources, with a scenario in which the shock compression of a flow provides an effective order to the otherwise random magnetic field, and thus increases not only the total and polarized fluxes, but also the percentage polarization; the same flow speed, orientation and compression are needed to independently reproduce the outburst strength, temporal profile, and percentage polarization; as shown by Aller et al. (2002), even highly oblique shock structures may yield the observed level of polarized emission due to shock compression, when allowance is made for relativistic aberration.
- Observed degree of polarization is usually a weak function of observing frequency; further, Jones (1988) argues that the absence of large circular polarization severely limits the distribution of low energy particles; there is a severe limit to the ability of Faraday effects to produce low levels of linear polarization, which is more likely to result from 'root-N' depolarization; recent work admits an ordered component of magnetic field (Beckert & Falcke 2002; Homan & Wardle 2004), but still requires a significant random component.
- First results from the MOJAVE project (Lister 2003) find enhanced magnetic field ordering at flow bends, where shear would be expected to be most influential in modifying an otherwise disordered magnetic field.
- Unless substantially beamed, Chandra and ASCA X-ray observations of kiloparsec scale jet-knots imply magnetic fields as much as four orders of magnitude in energy density below equipartition value (Kataoka & Stawarz 2004), dynamically unimportant, and subject to the dynamical influence of entrainment and the onset of turbulence.

Contrary to recent claims (Lyutikov et al. 2004) made in support of evidence for ordered parsec-scale jet fields, a continuous sequence of shocks is not needed to yield non-negligible interknot polarization. Indeed, hydrodynamic simulations, with the most minimal disturbance to the jet, reveal a complex web of weak oblique structures that can impose a degree of order consistent with the observed polarization: macroscopic propagating knots are then distinct features imposed on this underlying pattern, and their presence implies a spectrum of disturbances to the flow that simultaneously generate a degree of 'background' order.

Interesting structures (e.g., oblique shocks) may form in a simulated flow, but the response of a turbulent magnetic field to the formation of such structures is difficult to judge using conventional numerical RMHD methods, because an initially turbulent field injected with the jet material may have been subjected to other compressions and shear (providing a significant degree of order, which in a real flow might have been offset by entrainment or the spontaneous generation of turbulence in a high Reynolds number medium), before the structure of interest forms. To avoid such problems, epochs have been identified in our jet simulations, that span the formation and propagation of distinct structural features (such as oblique shocks); we have then made spatial and temporal cuts to isolate such evolving features, and used the corresponding velocity information to passively evolve initially turbulent field distributions.

The next three sections provide technical background; skip to the Conclusions to find out how the flow evolution influences magnetic field morphology, and thus the polarization structure of parsec-scale jet components.

Technicalities I: Hydrodynamics – Quite Shocking

The results presented below were obtained using the fully 3D, relativistic, hydrodynamic code for which the numerical method (RHLLE), tests, and first results were discussed in detail by Hughes et al. (2002). The only two modifications for the current application are as follows. First, the code has been adapted to run on a Linux cluster using CactusCode (http://www.cactuscode.org/), and shock-tube tests have been used to verify the integrity of the solver in this new environment: the run described here was performed on 16 processors. Second, 'pseudo-gravity' terms have been added to the solver, in order to maintain an initial pressure gradient in the ambient medium. The calculation assumes an inviscid and compressible gas, and an ideal equation of state with constant adiabatic index, Γ, and evolves mass density R, the three components of the momentum density M_x, M_y and M_z, and the total energy density E relative to the laboratory frame. Defining the vector (in terms of its transpose for compactness) $U = (R, M_x, M_y, M_z, E)^T$, and the three flux vectors

$$F^x = (Rv^x, M_x v^x + p, M_y v^y, M_z v^z, (E+p)v^x)^T, \quad (1)$$

$$F^y = (Rv^y, M_x v^x, M_y v^y + p, M_z v^z, (E+p)v^y)^T, \quad (2)$$

$$F^z = (Rv^z, M_x v^x, M_y v^y, M_z v^z + p, (E+p)v^z)^T, \quad (3)$$

where the three components of velocity are v^x, v^y and v^z, the conservative form of the relativistic Euler equation is

$$\frac{\partial U}{\partial t} + \frac{\partial}{\partial x}(F^x) + \frac{\partial}{\partial y}(F^y) + \frac{\partial}{\partial z}(F^z) = 0. \quad (4)$$

(The pressure, p, is given by the ideal gas equation of state in terms of the internal energy, e, and mass density, n, by $p = (\Gamma - 1)(e - n)$, and $c = 1$.) To model a gravitational field that maintains an arbitrarily imposed pressure gradient, a source term is added: of form $-(E+p)\,g$ to the M_z update, and of form $-M_z g$, where $g = -\nabla p/(e+p)$, to the E update. The effectiveness of this approach was easily tested, by noting the absence of evolution of an initial pressure gradient, in the absence of jet inflow, for a number of computational cycles comparable to that used in the final simulation.

The simulation discussed here spans 4480 computational cycles on a grid of extent $240 \times 240 \times 500$ cells; the lateral extent of the domain is ~ 10 jet-radii, and the longitudinal extent is ~ 21 jet-radii. Both jet and ambient medium are characterized by an adiabatic index $\Gamma = 4/3$, the inflowing jet has a (modest) Lorentz factor, $\gamma = 1.5$, a relativistic Mach number $\mathcal{M} = 4.3$, and an opening angle of 2 deg. A precessional perturbation of lateral velocity 0.05 and frequency 0.15 (in units set by inflow speed and jet radius) is applied to stimulate the development of normal modes of the cyclindrical flow. The ambient medium has a density at the inflow plane $10\times$ that of the jet, and declines with ambient pressure, corresponding to an isothermal atmosphere. Pressure in the ambient medium is initially equal to that of the inflowing jet material, and declines along the jet direction as $p(z) = p_0 \left(\frac{z}{zR_j+z_c}\right)^\beta$, where R_j is the jet radius, z_c is a scale height, taken here to be $5R_j$, and the power law index was taken to be 0.6 (Eilek, private communication).

Figure 1 shows the formation and evolution of an oblique shock in the body of the jet, from computational cycle 17520 to 22000. The physical time spanned by this stage in the flow's evolution is 9.8 jet-diameter light crossing times.

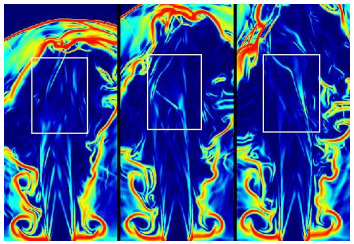

Figure 1.

Technicalities II: Field Evolution – Go With The Flow

An initially random magnetic field was generated by selecting random phases, and random amplitudes from a Rayleigh distribution, for the Fourier transform of the vector potential, $\tilde{\mathbf{A}}(\mathbf{k})$. The Fourier transform of the magnetic field is then $\tilde{\mathbf{B}}(\mathbf{k}) = i\mathbf{k} \times \tilde{\mathbf{A}}(\mathbf{k})$, and an inverse Fourier transform of this yields a magnetic field that is guaranteed to satisfy the divergence-free constraint. (See, e.g., Tribble (1991) for a detailed exposition of this approach.) By choosing a Gaussian form for the variance, $\sigma^2(k)$, in the Rayleigh distribution, the correlation scale can be controlled, and it was chosen to be 4 computational cells – 10% of the computational volume height; 'root-N' depolarization will then lead to a net polarization for the total emission from the volume of order a few percent, typical of the quiescent state of radio-loud AGN (Jones et al. 1985). Sufficient cells were pregenerated to allow field to be advected into the 'active' computational volume from below.

Within the volume indicated by the white rectangles on Figure 1 the magnetic field is advected according to the induction equation,

$$\frac{\partial \mathcal{B}}{\partial t} = \nabla \times (\mathbf{v} \times \mathcal{B}) + \eta \nabla^2 \mathcal{B}, \quad (5)$$

where η is the resistivity (the dissipative term being added for computational expediency – see below – by analogy with the nonrelativistic induction equation), and the field $\mathcal{B}$ relates to the spatial components of the magnetic four vector, $\mathbf{B}$, through $\mathbf{B} = \frac{\mathcal{B}}{\gamma} + \gamma(\mathcal{B}\cdot\mathbf{v})\,\mathbf{v}$, for Lorentz factor γ. For numerical purposes the induction equation is recast in integral form:

$$\frac{\partial}{\partial t}\int_\Sigma \mathcal{B}\cdot d\mathbf{S} + \oint_C (\mathcal{B}\times\mathbf{v} + \eta\nabla\times\mathcal{B})\cdot d\mathbf{l} = 0. \quad (6)$$

Discretization then yields algebraic equations for the updates to the average of the magnetic field over a surface, proportional to the discretization scales as $\Delta t/\Delta h$. The velocities are regarded as stored at cell centers, and the magnetic field components on cell faces – the surface for integration (the x-component on the higher x face of a voxel, etc.). The line integral thus becomes the sum of terms around face edges, and the velocity and magnetic field component values at the centers of these edges are derived by interpolation as needed. (See, e.g., Komissarov (1999) for a detailed exposition of this approach.) This technique preserves the divergence-free constraint to machine accuracy, but unfortunately does not conserve flux. It has been established by advecting a random field with a *uniform* velocity distribution, that by adding a small dissipation, $\eta \sim 0.085$, the global magnetic energy density does not grow, while the field remains random (as judged by the variance of the components) to within 15% at the mid-time in evolution, when structure of interest develops.

Figure 2 shows the fluid frame magnetic field components in a x = const plane (the same midplane as that shown in Figure 1) at 9 epochs during evolution by the pre-computed velocity field. In each panel the length of the lines is a measure of the average magnetic field in a 3^3 cube centered on the cut plane, and their maximum length is the same in each panel.

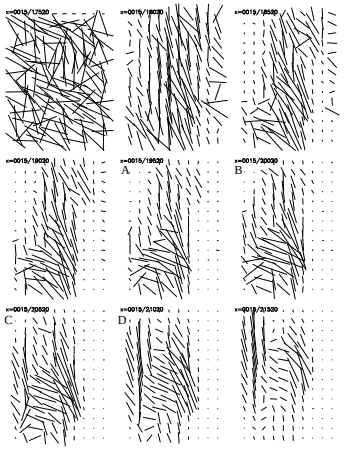

Figure 2.

Technicalities III: Radiative Transfer – A Transparent Argument

The transfer of polarized radiation through a diffuse plasma, allowing for emission, absorption, the birefringence effects of Faraday rotation and mode conversion (which can produce modest levels of circular polarization), and relativistic aberration and boost, has been described in detail by a number of authors. The analysis of Jones & O'Dell (1977) is followed; this is compactly summarized by Jones (1988), and has been used previously in the study of parsec-scale jets; see, for example, Hughes et al. (1989a) and Gómez et al. (1993).

A full radiative transfer requires some knowledge of the particle distribution function: the low energy cutoff Lorentz factor, the Lorentz factor of particles radiating at the observer frequency, and the frequency spectral slope of the distribution; these are arbitrarily fixed at $\gamma_{a0} = 100$, $\gamma_{n0} = 1000$, and $\alpha = 0.75$. For the results presented below, values were chosen to yield an optically thin flow. Observations strongly suggest that the particle distribution and magnetic field, jointly responsible for the synchrotron radiation, are confined to the inflowing jet, and do not permeate the ambient medium. To model this, a filter is applied, so that no emission arises from cells with velocity $v < v_{\rm crit} = 0.5$ ($c = 1$). In principle, the radiative transfer should use retarded times; that has not been done in the results shown below, but this will have minimal impact on the validity of the results, as individual features move rather slowly.

Figure 3 shows, from upper-left to lower-right, 'fake' maps of polarized intensity, spanning the 5th through 8th epochs shown in Figure 2, computed for an observer orientation corresponding approximately to the view through the midplane of the computational volume shown in Figure 2. Care must be taken in comparing Figure 2 with Figure 3: the former is a slice through a computational volume, whereas the latter shows an integration along lines of sight. The intensity pattern on the plane of the sky has been convolved with a 10-pixel Gaussian beam – corresponding to four beam widths across the shock structure of interest, and typical of the best VLBI resolutions now being attained for parsec scale jets. The scaling has been chosen so that the maps have comparable dynamic range.

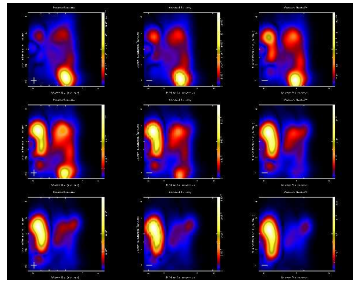

Figure 3.

The localized peak in intensity in the first panel of Figure 3 is offset from the regions of most-ordered field at that epoch – associated with the shock above, and shear at right – seen in the central panel of Figure 2, because that line-of-sight intersects regions of ordered field and high pressure not revealed by the simple center-plane cut of Figure 2. Careful exploration of the flow structure shows that what appears to be a simple, oblique shock, does indeed comprise thin, approximately planar features oblique to the flow direction, but that there are two nested discontinuities, which curve slightly to follow the local jet boundary, extending for about one-third of the jet circumference, and converging at their base on the flow edge.

The devil is in the detail, and in this case, the devil is in the knot of emission. Even the simplest of VLBI structures may be hiding a complex flow pattern. Subsequent evolution leads to a weak feature downstream of the initial bright knot, reflecting the increasing influence of emission from both the downstream flow of the shock 'complex', and the shear at the jet edge above this, and, finally, another distinct knot associated with the region of strong shear that arises as the jet direction changes. This simulation is applicable to the interpretation of sources with relatively short-lived components, such as some BL Lac objects, with variable apparent speed and/or nonlinear trajectories (Denn et al. 2000). It is interesting to see that an asymmetric shear layer is easily produced, which might have relevance for the interpretation of VLBI features suggestive of the presence of a flow boundary (Attridge et al. 1999), and it clearly warns against the naive interpretation of observations that reveal knots that seemingly abruptly change direction and decelerate.

Conclusions

- **Evolution of simple internal jet structures and shear layers can lead to behavior mimicing the evolution of a single component with complex dynamics.**
- **The domains dominated by shear at the jet edge are not static, and evolve as the jet shifts laterally. Thus, in the example above, under low resolution it would appear that a region of transverse field evolved into a region of longitudinal field; higher resolution might suggest that a component within the flow propagates along a somewhat curved trajectory, with a rotation of the plane of polarized emission towards the longitudinal sense.**
- **Non-linear trajectories and a rotation of the plane of polarization as a component evolves may be manifestations of evolution *within* a channel broader than that suggested by the data.**
- **Evolving, complex, internal structure, does not necessarily result from the interaction of the jet with ambient density or pressure structures, but, rather, may form and evolve due to the response of the jet to small perturbations.**
- **Defining the dynamics of such flows through VLBI observations demands a sequence of maps with high time resolution, and of sufficient duration to probe the global structure of the flow. Isolated epochs may reveal transient peculiarities, not representative of the overall flow morphology.**

Keeping It Legal

This work was supported in part by NSF grant AST 0205105. The author thanks Hugh and Margo Aller for illuminating discussions on the observational implications of the study. Comer Duncan and Mark Miller have made major contributions to the hydrodynamic simulations.

Aller, H. D., Aller, M. F., & Hughes, P. A. 2002, Proceedings of the 6th European VLBI Network Symposium, ed. E. Ros, R. W. Porcas, & J. A. Zensus, (Bonn, Germany: MPIFR), 111

Attridge, J. M., Roberts, D. H., & Wardle, J. F. C. 1999, ApJ, 518, L87

Beckert, T., & Falcke, H. 2002, A&A, 388, 1106

Denn, G. R., Mutel, R. L., & Marscher, A. P. 2000, ApJS, 129, 61

Gómez, J. L., Alberdi, A., & Marcaide, J. M. 1993, A&A, 274, 55

Gómez, J. L., Alberdi, A., & Marcaide, J. M. 1994a, A&A, 284, 51

Gomez, J.-L., Alberdi, A., Marcaide, J. M., Marscher, A. P., & Travis, J. P. 1994b, A&A, 292, 33

Homan, D. C., & Wardle, J. F. C. 2004, ApJ, 602, L13

Hughes, P. A., Aller, H. D., & Aller, M. F. 1989a, ApJ, 341, 54

Hughes, P. A., Aller, H. D., & Aller, M. F. 1989b, ApJ, 341, 68

Hughes, P. A., Aller, H. D., & Aller, M. F. 1991, ApJ, 374, 57

Hughes, P. A., Miller, M. A., & Duncan, G. C. 2002, ApJ, 572, 713

Jones, T. W. 1988, ApJ, 332, 678

Jones, T. W., & O'Dell, S. L. 1977, ApJ, 214, 522

Jones, T. W., et al. 1985, ApJ, 290, 627

Kataoka, J., & Stawarz, L. 2004, astro-ph/0411042

Komissarov, S. S. 1999, MNRAS, 303, 343

Lister, M. L. 2003, astro-ph/0309413

Lyutikov, M., Pariev, V. I., & Gabuzda, D. C. 2004, astro-ph/0406144

Tribble, P. C. 1991, MNRAS, 253, 147

This miniposter was prepared with Brian Wolven's Poster LaTeX macros v2.1.

Fig. 1.—

Fig. 2.—

Fig. 3.—